

Heat conduction calorimeter for massively parallel high throughput measurements with picoliter sample volumes

E. B. Chancellor, J. P. Wikswo, and F. Baudenbacher^{a)}
Vanderbilt University, Nashville, Tennessee 37212

M. Radparvar and D. Osterman^{b)}
Hypres Inc., Elmsford, New York 10523

(Received 9 June 2004; accepted 16 July 2004)

We have developed a bulk micromachined calorimeter with a sensitivity of $1.5 \text{ nW/Hz}^{1/2}$ and a 1 ms time constant using a thin film thermopile as the sensing element. The thermopile consists of seven titanium and bismuth thermocouples with a total Seebeck coefficient of $574 \mu\text{V/K}$. The device is capable of measuring enthalpies in chemical or biological reactions in volumes as small as a few picoliters. The device can be fabricated and operated in a massively parallel fashion in combination with ink-jet printing technologies in air and at room temperature, making it ideally suited for biological and biochemical experiments. © 2004 American Institute of Physics.
 [DOI: 10.1063/1.1790075]

Microcalorimetry is generally used to measure enthalpy changes during phase transitions, chemical reactions, or biological and biochemical processes.^{1–3} In the last decade, micromachining has been used to reduce the sample volumes and increase the sensitivity of calorimetric measurements.^{4,5} Zhang *et al.* describe a calorimeter using a silicon nitride (SiN) membrane and a thin film nickel resistor to detect the temperature changes generated by the sample.⁶ The SiN membrane has also been used in conjunction with a differential thermopile to measure the heat generated by the catalase activity of single hepatocyte cells by Johannessen *et al.*,⁷ who used 10 Ni/Au thermocouples with a total Seebeck coefficient of $220 \mu\text{V/K}$.

In this letter we describe an optimized micromachined calorimeter, with a sensitivity that is higher than previously reported and a time constant on the order of 1 ms, which is suitable for high throughput measurements using ink-jet printing technologies to deliver nanoliter and picoliter volumes to an array of devices.⁸ This will allow hundreds or thousands of experiments to be conducted rapidly and simultaneously, whether for titration experiments,⁹ controlled denaturation of proteins and other biomolecules, or determining the differences in binding kinetics¹⁰ and affinities of a large library of chemicals or well-defined sets of related molecules created by site-directed mutagenesis.¹¹ The small sample volume reduces reagent costs, conserves valuable and difficult-to-obtain biomolecules, and provides a measurement bandwidth that cannot be achieved with microcalorimeters that have larger thermal masses.

The fabrication of the calorimeter starts with the transfer of a computer aided design to a chrome-on-quartz mask, which was used for the photolithographic pattern definition step. We started with a 3 in. Si substrate covered on both sides with amorphous SiN, a material that is strong enough to fabricate free standing membranes of submicrometer thickness. The critical micromachining steps are imple-

mented as follows: a square opening is etched, by reactive ion etching, in the amorphous SiN film on the back of the wafer. The wafer is then immersed in a liquid potassium hydroxide etchant that attacks Si but does not etch SiN. Furthermore, the etchant acts anisotropically, faster in the [100] direction and slower in the [110] direction, which, for a (100) Si wafer, results in a pit with inward slanting walls. The SiN layer acts as an etch stop and forms the bottom of the pit. As a result, a rigid SiN membrane remains, suspended over an opening in the wafer. The first thermopile electrode is evaporated onto the SiN membrane using electron beam evaporation and consists of a Ti and Au bilayer. After patterning this bilayer, vias in the Au film are defined for the Ti/Bi thermopile junctions. Then a layer of Bi is deposited as the second electrode, and finally the Au is removed from the Au/Ti bilayer. Figure 1(a) shows the resulting device with seven thermocouples. The right-hand pads in Fig. 1(a) are connected to a resistive heater in the center of the device, used for calibration and for differential scanning calorimetry measurements.

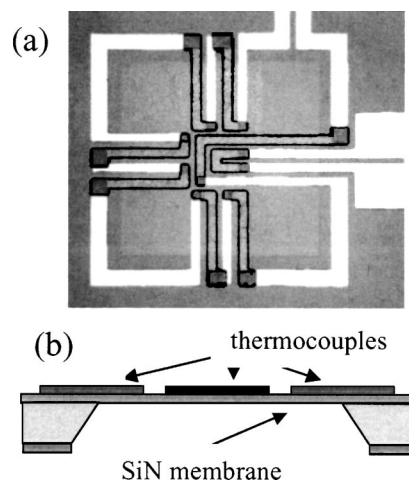


FIG. 1. (a) Photograph of a heat conduction calorimeter with seven thermocouples and an integrated resistive heater. (b) Cross-sectional view of the calorimeter.

^{a)}Author to whom correspondence should be addressed; electronic mail: F.Baudenbacher@Vanderbilt.edu

^{b)}Present address: Ball Aerospace & Technology Corp., Boulder, Colorado, 80306.

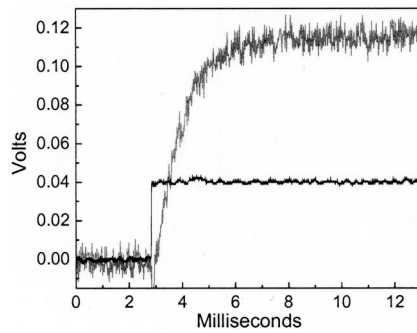


FIG. 2. Dynamic properties of the calorimeter. The black trace is a square-wave voltage applied to the integrated resistive heater. The grey trace is the voltage generated by the thermopile of the calorimeter.

As a first step we evaluated the response of the calorimeter to a heat pulse deposited on the membrane using the integrated heater. The voltage across the heater (black trace) and the voltage generated by the thermopile (grey trace) are displayed in Fig. 2. These measurements allowed us to determine simultaneously both the responsivity and the time constant of the calorimeter: 6.34 V/W and 1 ms, respectively.

The spectral noise density, measured using a custom designed low-noise preamplifier and an HP 3562A spectrum analyzer, was 10 nV/Hz^{1/2} at 0.1 Hz and showed no components other than the Johnson noise of the thermopile resistance. This measurement, divided by the power responsivity, yields a power sensitivity of 1.5 nW/Hz^{1/2}. The voltage noise can be converted to a temperature taking into account the number of thermocouples and a Seebeck coefficient of 82 V/K for each Bi/Ti thermocouple. The equivalent noise would be 17.42 μ K/Hz^{1/2} for a seven thermocouple device.

The responsivity of our calorimeter changed with operating temperature at a rate of 0.14% per °C over the temperature range from -20 to 70 °C. Therefore, this device can be used over a wide temperature range with only small corrections necessary.

We designed our calorimeter for measuring enthalpy changes in chemical and biological reactions with ink-jet printing technologies used to deliver picoliter volumes to the reaction chamber. To demonstrate feasibility, we used a commercially available microdispenser to deposit 1–500 pl water droplets to the calorimeter surface. Figure 3 shows the heat consumption due to the evaporation of a 225 pl drop of water.

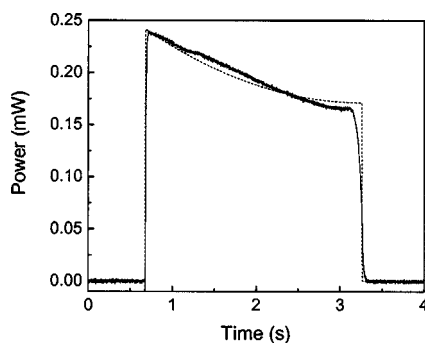


FIG. 3. Power consumption by a 100 pL water droplet as it evaporates (solid line), along with the fit from our single parameter model (dashed line).

The thermovoltage generated by the thermopile is given by $V = n \cdot S \cdot \Delta T$, where ΔT is the temperature difference across the thermopile, n the number of thermocouples, and S the Seebeck coefficient. In order to predict the power generated by an evaporating water droplet, we developed a simple model in which heat flows from the substrate into the water droplet. We assumed that all heat flowing into the water will go toward evaporation and temperature change, and that there is no heat exchange with the environment. According to these assumptions the energy conservation law can be written as

$$C \frac{d\Delta T}{dt} + K \cdot \Delta T = \ell \frac{dm}{dt} + c \frac{dm}{dt} \Delta T + c \cdot m \frac{d\Delta T}{dt}, \quad (1)$$

where $\Delta T(t)$ is the thermopile temperature gradient, C the heat capacity and K the thermal conductance of the SiN membrane and the metal films of the thermopile, $m(t)$ the mass of the water droplet, L the latent heat of evaporation of water at room temperature, and c the specific heat of water. To model the time course of the drop evaporation, we assumed a spherical cap shape, and let the cap height go to zero linearly while the radius of the drop remains constant. This model for droplet evaporation is accurate down to contact angles of about 7°, after which the radius also begins to shrink.¹² The equations for $m(t)$ and dm/dt are then

$$m(t) = \left(\frac{\rho\pi}{6} \right) \left[3r^2h_0 \left(1 - \frac{t}{t_0} \right) + h_0^3 \left(1 - \frac{t}{t_0} \right)^3 \right], \quad (2)$$

$$\frac{dm}{dt} = - \left(\frac{\rho\pi}{2t_0} \right) \left[r^2h_0 + h_0 \left(1 - \frac{t}{t_0} \right)^2 \right], \quad (3)$$

where ρ is the density of water, r is the radius of the drop, h_0 the initial height of the drop, t the time, and t_0 the time interval required for the water drop to evaporate. In order to fit the model to the data, we substituted Eqs. (2) and (3) into Eq. (1) and solved the system numerically. To obtain the best fit we let h_0 , t_0 , and the ratio h_0/r be parameters in a least-squares curve fit. Initial estimates of these parameters were taken from high speed video images. Figure 3 shows the comparison of the actual data and the results of our heat-flow model, confirming the validity of our approach. The fit shows deviations only at small droplet volumes, which are most likely due to uneven evaporation at small contact angles.

Figure 4 shows a plot of the experimentally determined heat of evaporation versus mass for sixteen drops recorded with our device. The heat is obtained by integration of the calorimeter signal, and the mass is obtained from the model fit that provides the latent height and radius. The slope of the line represents the latent heat of evaporation of water. From our data we obtained 2263 kJ/kg as the latent heat, which compares relatively well with the bulk value of 2443 kJ/kg at 25 °C.¹³ We attribute the difference due to an oversimplification in the droplet shape¹² and heat loss into the environment, which is not accounted for in the model.

The power sensitivity of the device discussed, at a level of 1.5 nW/Hz^{1/2}, will be sufficient to measure processes in pL sample volumes. Our calorimeter has a measured time constant of 1 ms, over one order of magnitude faster than AIP license or copyright, see <http://apl.aip.org/apl/copyright.jsp>

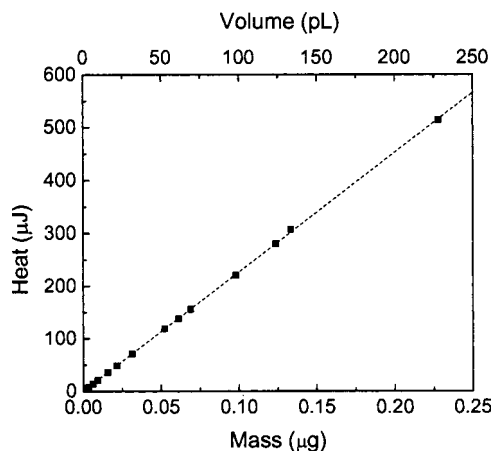


FIG. 4. The experimentally determined heat of evaporation vs mass (lower *x*-axis) and volume (upper *x*-axis) for sixteen 1 to 500 pL water drops recorded by our calorimeter (■) and a least-squares fit to the data (dashed line). The slope of the fit represents the latent heat of water at room temperature.

that of similar instruments.¹⁴ Furthermore, this time constant, coupled with the nanowatt sensitivity, is obtained for operation in ambient air. Ink-jet printing technologies combined with arrays of high sensitivity calorimeters using such small

volumes will increase dramatically the throughput in calorimetric measurements.

This work was supported in part by NIH Grant No. 1 R43 RR16157-01 and by the Vanderbilt Institute for Integrative Biosystems Research and Education. The authors thank Hassane Mchaourab and Joel Tellinghuisen for helpful discussions.

¹K. P. Murphy and E. Freire, *Adv. Protein Chem.* **43**, 313 (1992).

²I. Wadso, *Thermochim. Acta* **394**, 305 (2002).

³I. Wadso, *J. Therm. Anal. Calorim.* **64**, 75 (2001).

⁴S. L. Lai, J. Y. Guo, V. Petrova, G. Ramanath, and L. H. Allen, *Phys. Rev. Lett.* **77**, 99 (1996).

⁵D. W. Denlinger, E. N. Abarra, K. Allen, P. W. Rooney, M. T. Messer, S. K. Watson, and F. Hellman, *Rev. Sci. Instrum.* **65**, 946 (1994).

⁶M. Zhang, M. Y. Efremov, E. A. Olson, Z. S. Zhang, and L. H. Allen, *Appl. Phys. Lett.* **81**, 3801 (2002).

⁷E. A. Johannessen, J. M. R. Weaver, L. Bourova, P. Svoboda, P. H. Cobbold, and J. M. Cooper, *Anal. Chem.* **74**, 2190 (2002).

⁸E. R. Lee, *Microdrop Generation* (CRC Press, Boca Raton, FL, 2003).

⁹J. E. Ladbury, *Thermochim. Acta* **380**, 209 (2001).

¹⁰T. T. Waldron and K. P. Murphy, *Biochemistry* **42**, 5058 (2003).

¹¹H. Ohtaka, A. Schon, and E. Freire, *Biochemistry* **42**, 13659 (2003).

¹²M. diMarzo and S. Tinker, *Fire Saf. J.* **27**, 289 (1996).

¹³*CRC Handbook of Physics and Chemistry* (CRC Press, Boca Raton, FL, 2004).

¹⁴E. A. Johannessen, J. M. R. Weaver, P. H. Cobbold, and J. M. Cooper, *Appl. Phys. Lett.* **80**, 2029 (2002).